Electro-Thermal Modeling of Fuel Cells and Batteries for CHEETA Aircraft

Meaghan Podlaski[1,2], Abhijit Khare [1,3], and Luigi Vanfretti [1]
[1] *Department of Electrical, Computer, and Systems Engineering, Rensselaer Polytechnic Institute, Troy, NY, USA*
{podlam, vanfrl}@rpi.edu
[2] *General Electric Vernova Research, Niskayuna, NY, USA*
[3] *General Electric Renewable Energy, Schenectady, NY, USA*
abhijit.khare@ge.com

I. Nomenclature

BMS	=	Battery management system
CHEETA	=	Cryogenic High-Efficiency Electrical Technologies for Aircraft
EMS	=	Energy management system
FMI	=	Functional mock-up interface
FMU	=	Functional mock-up unit
HTS	=	High temperature super-conducting transmission line/cable
PEMFC	=	Proton-exchange membrane fuel cell
SOFC	=	Solid oxide fuel cell

II. Introduction

A. Background

In the development of novel electrified aircraft concepts such as the CHEETA aircraft [1], well-defined models representing multiple physical and engineering domains are useful in completing aircraft sizing and trade-off studies in different simulation environments. In the design stages of such types of aircraft, there are limited opportunities for testing and building physical prototypes of this aircraft concept, and thus, simulation studies give insight into which designs have the most benefit [2].

Since the CHEETA aircraft system is in an early stage of system development, integrated simulation studies of multi-physics models assist in subsystem design and parameter definition [3]. In this work, multi-physics models of the aircraft's fuel cell and battery are developed. These models are then studied to understand their dynamic electro-thermal behavior, providing additional information on design considerations in early system development stages.

B. Related Works

First-principles, multi-domain modeling techniques have assisted in modeling other electric aircraft such as [4] and [5]. These works serve as a foundation for the development of a multi-physics electric aircraft model using the Modelica modeling language; however, these projects do not use fuel cells and batteries as the aircraft's primary power source or cryogenic cooling throughout the system. Both works use a similar modeling structure to the one used with CHEETA, where the models are able to be easily configured at different levels of modeling fidelity to perform a wide range of trade studies and enhance simulation predictive capabilities [3].

The work presented herein focuses on the development of electro-thermal models for the fuel cell, battery, and their controls as envisioned for the CHEETA aircraft power system. Since both the electrical and thermal domains are represented in the fuel cell and battery models, simulation studies can be used to understand how these components interact with the rest of the aircraft's power system. The system architecture has been previously defined in [1]; the multi-domain models for other subsystems such as the high-temperature superconducting (HTS) cables are described in [6].

C. Paper Contributions

The main contributions of this work are:

- Definition of electro-thermal battery and fuel cell models that have been validated against experiment data.
- Simulation studies to understand battery cold plate design with respect to electrical losses and dynamic response.

D. Paper Overview

An introduction to the CHEETA electrical and thermal system is provided in Section III. The fuel cell electro-thermal model is discussed in Section IV. Simulation studies for the fuel cell integrated into the remainder of the CHEETA aircraft power system are also included in this section. The battery model is discussed in Section V, where the eletro-thermal model is studied under different cold-plate operating conditions to understand how the thermal system design affects the battery's electrical dynamics and losses.

III. CHEETA Aircraft Overview

The CHEETA aircraft is a fully-electric aircraft powered by a series of hydrogen fuel cells and batteries. The aircraft's electrical system operates at 20° K, as it is cooled by liquid hydrogen at cryogenic temperatures to minimize losses. As a result, it is necessary to develop component and system models that are able to represent multiple physics behaviors such as electrical, thermal, mechanical, and control. The aircraft's electrical architecture is shown in Figure 1, where it has a hybrid centralized and distributed architecture. The aircraft is powered by a series of fuel cells and batteries, making it necessary to have detailed, accurate models of the sources. The fuel cells are connected in a centralized configuration, with tie-line connecting the three fuel cell generation buses. The power produced by the fuel cells are carried to the motors via HTS transmission line. Each bus where the motors are connected also has a battery that provides extra power during periods of high energy consumption such as take-off and is the sole power source during taxiing. More information on the system architecture and HTS lines can be found in [1, 6]. Other subsystems in the CHEETA system have been modeled according to a multi-domain behavior, such as with the HTS transmission lines [6]. Sizing studies have also been conducted for this specific aircraft configuration in [7] to assist in the defining system requirements from a propulsion perspective.

Each component in the electrical system is modeled in both the electrical and thermal domains, which enables integrated trade-off studies and sizing analysis. Figure 2 shows the relationship between the various domains in one branch of the electrical system in Figure 1, where the electrical, thermal, mechanical, and control domains are represented. In this work, the term 'domain' refers to each specific physical behavior of interest or engineering field. For example, all electrical variables in these models are connected and obey fundamental principles such as Ohm's Law and Kirchoff's Laws. The thermal domain is modeled in each component such that all variables and equations obey the laws of thermodynamics. Integrating each electrical and thermal behavior together within a component and system model realizes a 'multi-domain' model, which allows to understand the interactions between domains.

The components of the power system in Figure 2 are labeled as follows:

(A) Fuel cell
(B) Battery
(C) Drivetrain system
    (1) Controller
    (2) Pulse width modulation
    (3) DC/DC converter
    (4) Motor
(D) HTS transmission line
(E) Propulsion fans
(F) Liquid hydrogen cooling system
(G) Main control unit/system controls

IV. Fuel Cell Subsystem Development

A. Model Development

In the CHEETA aircraft power system, the fuel cell uses proton exchange membrane (PEM) technology due to its operating temperature, power density, and the maturity of its chemical technology. After conducting initial sizing

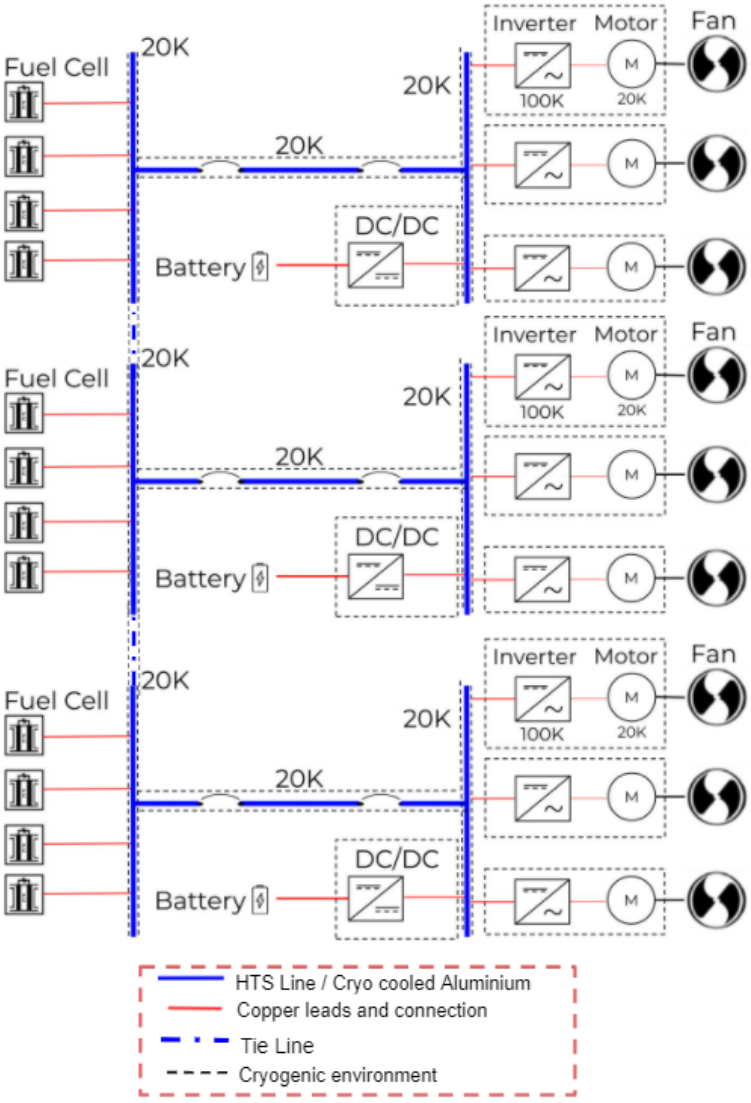

Fig. 1 CHEETA electrical system architecture.

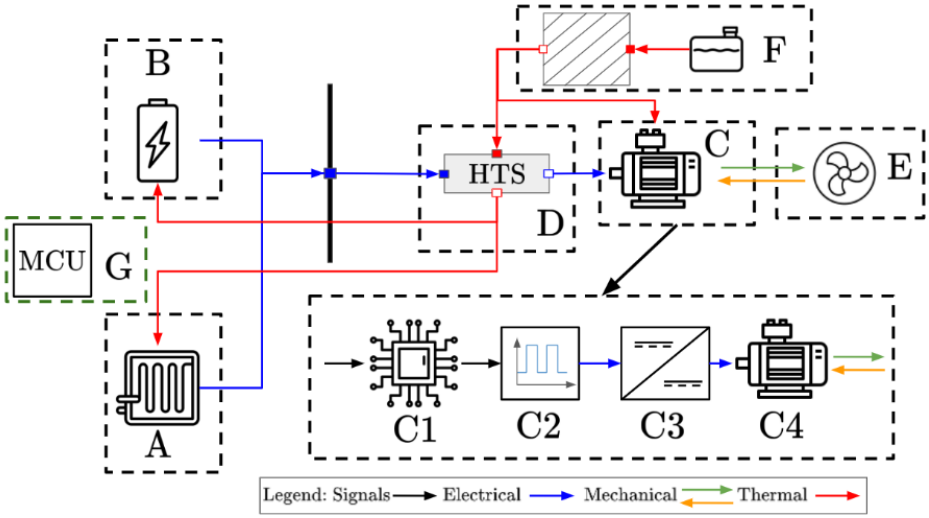

Fig. 2 Single branch of aircraft architecture demonstrating the relationships between the domains and subsystems.

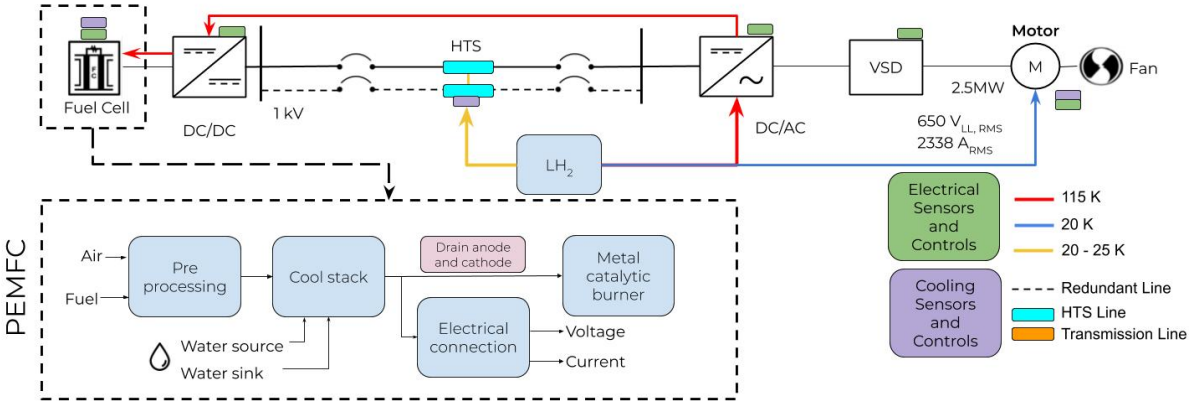

Fig. 3 Power system with fuel cell operations and functionalities shown in detail.

studies on the system in [1], the PEM fuel cell was deemed the best technology for the aircraft as it would not require a DC/DC converter linking the fuel cell to the rest of the system. This results in a lower system weight and reduced complexity in converter controls coordination.

The fuel cell models are derived from [8, 9] to define a mathematical model of a PEM fuel cell. This mathematical model is defined in the electrical and thermal domains, enabling integration and interaction with both the electrical and cryogenic cooling systems. Figure 3 shows the case of the PEM fuel cell operating with the powertrain, where the fuel cell processing sub-loop is based off of [8]. The block at the bottom of the diagram that expands upon the processes needed to transform the LH_2 to DC power [8, 10].

The electrical schematic of the PEM fuel cell model is shown in Figure 4, which consists of a cell voltage denoted as E_{cell} and multiple resistances and capacitors. The activation resistance R_{act} is determined by Equation 1, which is used to determine the voltage drop in the fuel cell due to activation. The resistance representing the concentration losses of the fuel cell is determined by Equation 2. These two resistances can be used to calculate losses caused by the chemical reactions in the fuel cell according to Figure 5. These losses vary as a function of the operating temperature T_f and current draw I_{FC} of the fuel cell. In Equations 1 and 2, R is the universal gas constant, α is the electron transfer coefficient, F is the Faraday constant, n_e is the number of electrons, and I_{max} is the maximum fuel cell current.

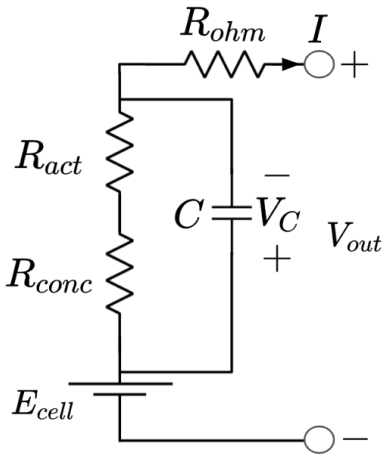

Fig. 4 PEM fuel cell electrical schematic.

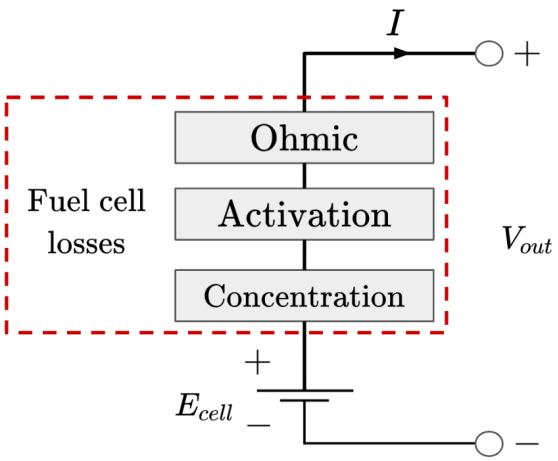

Fig. 5 Electrical losses in the fuel cell.

$$R_{act} = -\frac{RT_f \ln(I_{FC})}{\alpha n_e F I_{FC}} = \frac{V_{act,2}}{I_{FC}} \tag{1}$$

$$R_{conc} = -\frac{RT_f}{n_e F I_{FC}} \ln\left(\frac{-I_{FC}}{I_{max}}\right) \tag{2}$$

The fuel cell is also subject to ohmic losses in addition to activation and concentration losses. This is denoted in Figure 4 as R_{ohm}, which can be determined by Equation 3. These losses correspond to the electrical losses in the fuel cell, which can be caused by the electrical wiring and connection to the rest of the system. In Equation 3, R_{ohm0} is the constant portion of R_{ohm}, k_{RI} is an empirical constant for calculating R_{ohm} as a function of current, and k_{RT} is an empirical constant for calculating R_{ohm} as a function of temperature.

$$R_{ohm} = R_{ohm0} + k_{RI} I_{FC} - k_{RT} T_f \tag{3}$$

The output voltage of the fuel cell can be determined using the calculated activation, concentration, and ohmic losses according to Equation 4. The activation voltage is described empirically by the Tafel equation in Equation 5; this voltage drop is only dependent on the fuel cell's internal temperature. In Equation 6, η_0 is the temperature invariant part of the activation voltage, which is measured in Kelvin. The terms a_{FC} and b_{FC} in Equations 6 and 7 are constant terms used in the Tafel equation. The voltage drop across the capacitor in Figure 4 can be determined from Equation 8.

$$V_{out} = E_{cell} - V_c - V_{ohm} - V_{act1} \tag{4}$$

$$V_{act} = \eta_0 + (T_f - 298)a_{FC} + T_f b_{FC} \ln(I_{FC}) \tag{5}$$

$$V_{act1} = \eta_0 + (T_f - 298)a_{FC} \tag{6}$$

$$V_{act2} = T_f b_{FC} \ln(I_{FC}) \tag{7}$$

$$V_C = (I_{FC} - C\frac{dV_C}{dt})(R_{act} + R_{conc}) \tag{8}$$

The fuel cell's parameters are listed in Table 1. The parameters were derived from [10, 11] and scaled from the system requirements for CHEETA as necessary. The fuel cell has a power capacity of 2.5MW, operates at 1000V, and is parameterized with the stack values for the SR-12 stack from [10].

B. Model Validation and Simulation Studies

The model in [10] was originally modeled in Simulink, enabling us to re-implement the model using Modelica. The model developed using Modelica is imported in Simulink as a functional mock-up unit (FMU) [12], which is an open access standard that provides a model-sharing protocol that enables both models to be simulated in the same environment for validation. The fuel cell system is parameterized using the values in Table 1 and is configured with anode pressure $P_{anode} = 1.5$, cathode pressure $P_{cathode} = 1.0$, room temperature $T_{room} = 307.7°$ K, and initial

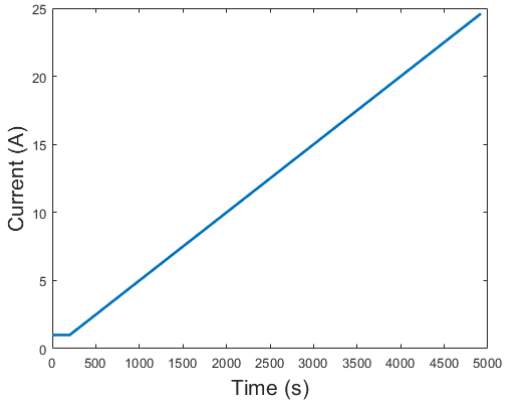

Fig. 6 Fuel cell current input for model validation.

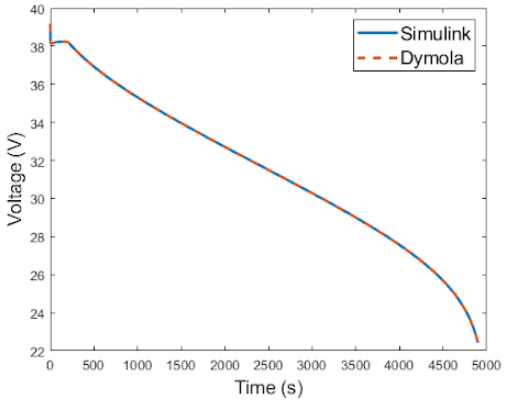

Fig. 7 Fuel cell voltage comparison for model validation.

temperature $T_{initial}$ = 307.7° K. The fuel cell model can be obtained from [13] and validated using an input current profile played back from the original Simulink model simulation data. The input current profile is shown in Figure 6. The voltage output of both the Simulink and Modelica models is shown in Figure 7. Both model voltage outputs match each other completely, thus validating the Modelica model.

This validated model is implemented using Modelica in the Dymola development environment [14], as shown in Figure 8. The inputs of the model are replaced with multi-domain connections to integrate the model with the electrical and thermal systems. The thermal connections are denoted by the red blocks `Troom` and `Tout`, which specify the temperature of the cooling medium and the operating temperature of the fuel cell respectively. These connections communicate the temperature and heat flow with the rest of the thermal system. The blue block `Vout` connects the output voltage of the fuel cell to the rest of the electrical system, communicating both a current and voltage value with other electrical components.

The fuel cell in Figure 8 is integrated into a test system consisting of the HTS transmission line, cooling system, and a single drivetrain that has been scaled to the same power level as the fuel cell. The scaling is necessary as parameters corresponding to the planned 2.5 MW fuel cell are not currently available. The system schematic is shown in Figure 9. The drivetrain is given a speed command of 100 rad/sec with a constant 200 N·m torque to test the fuel cell in a steady state, resembling a cruise flight behavior. The fuel cell current and voltage are shown in Figure 10 when the system is simulated under the previously defined conditions, where both properties remain constant after initialization.

V. Battery Subsystem Development

A. Model Development

In the CHEETA aircraft power system, the battery has a Li-Ion chemistry and is sized to provide extra power to the system during taxi, take-off, and landing as well as emergency power in the event of component failure within the fuel cell or HTS transmission systems. The battery models are derived from [15–17] to represent both the electrical and thermal behavior. The battery model is table-based, meaning all electrical and thermal characteristics correspond to values in a look-up table stored in the model. These look-up tables evaluate the temperature and state of charge (SoC) to determine the voltage and current produced by the battery. The table values were determined from a set of experiments conducted on the battery in [15, 17], providing a validated battery model when a physical prototype of the system is not available.

The battery system consists of the battery, a cold plate, a battery management system, and a DC/DC converter, as shown in Figure 11. The thermal domain is denoted by the red lines, the electrical by the blue lines, and the control schema by the black lines. The charging, discharging, and idle current of the battery are controlled by a bi-directional DC/DC converter. The operational state of this converter is controlled by the battery management system (BMS), which provides a signal denoting the duty cycle. The cold plate controls the temperature of the battery cells, which will change the electrical properties of the battery such as the internal impedance.

The battery system in Figure 12 is implemented in Dymola using the Modelica programming language. The model

Table 1 Fuel cell parameters.

Parameter	Description	Value
a_{FC}	Constant used in Tafel equation (V/K)	-0.1373
b_{FC}	Constant used in Tafel equation (V/K)	N/A
C	Fuel cell capacitance (F)	10.6
E_{cell}	Total cell voltage (V)	1558.9
F	Faraday constant(sA/mol)	96485.3321
k_{RI}	Empirical constant to calculate R_{ohm} (Ω/A)	1e-9
k_{RT}	Empirical constant to calculate R_{ohm} (Ω/A)	1e-9
I_{max}	Maximum fuel cell current (A)	5000
n_e	Number of electrons (mol)	2
PO_2	Partial pressure of oxygen (unitless)	1.6
PH_2	Partial pressure of hydrogen (unitless)	1.5
R	Universal gas constant ($J/molK$)	8.3145
$R_{ohm,0}$	Constant portion of R_{ohm} (Ω)	0.2793
T_f	Fuel cell temperature (K)	193
α	Electron transfer coefficient (unitless)	0.1373
η_0	Temperature invariant part of V_{act} (V)	20.145

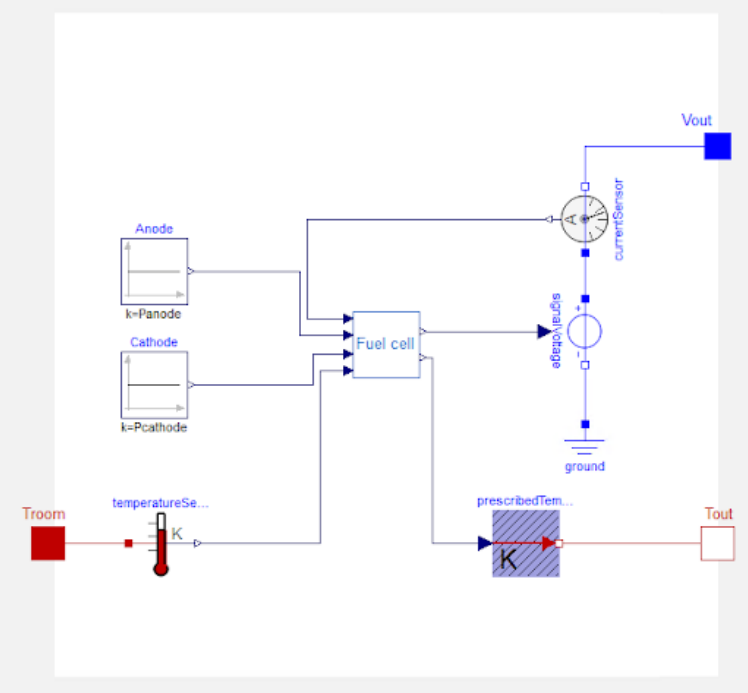

Fig. 8 Multi-domain fuel cell model in Dymola.

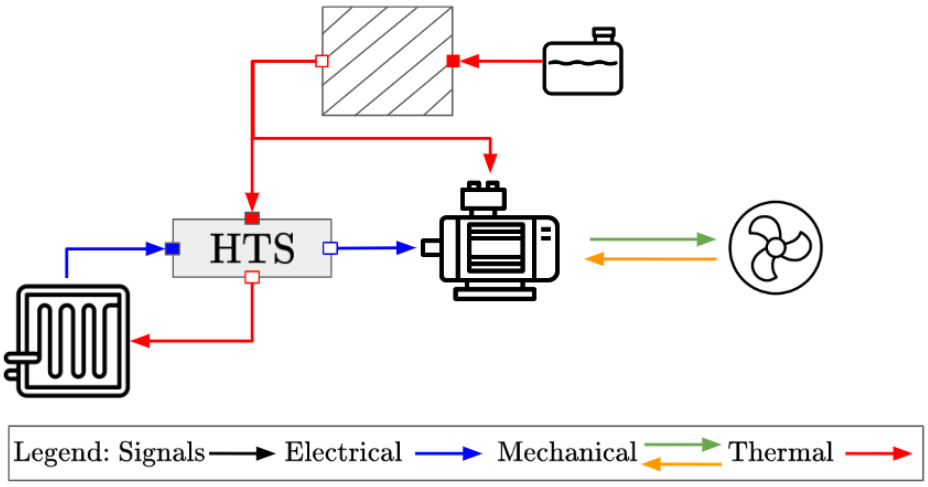

Fig. 9 Fuel cell and drivetrain test system schematic.

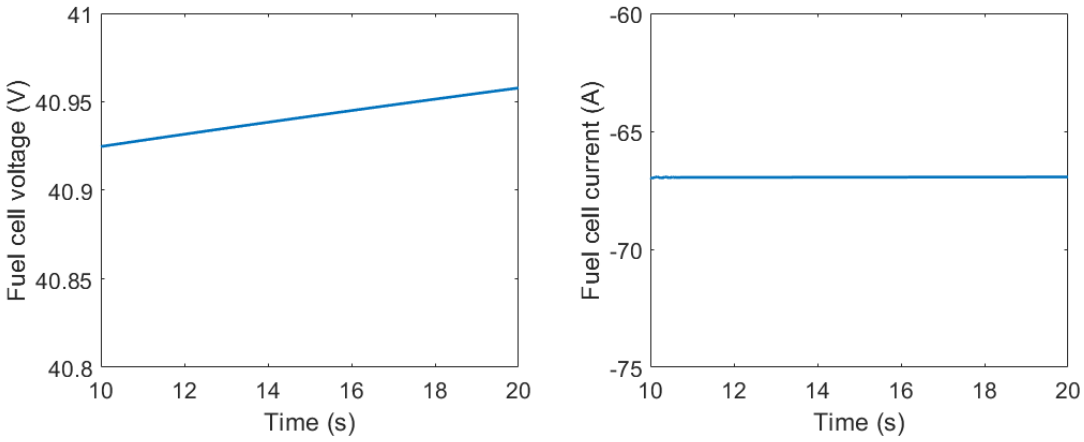

Fig. 10 Fuel cell current and voltage when connected to drivetrain in steady state.

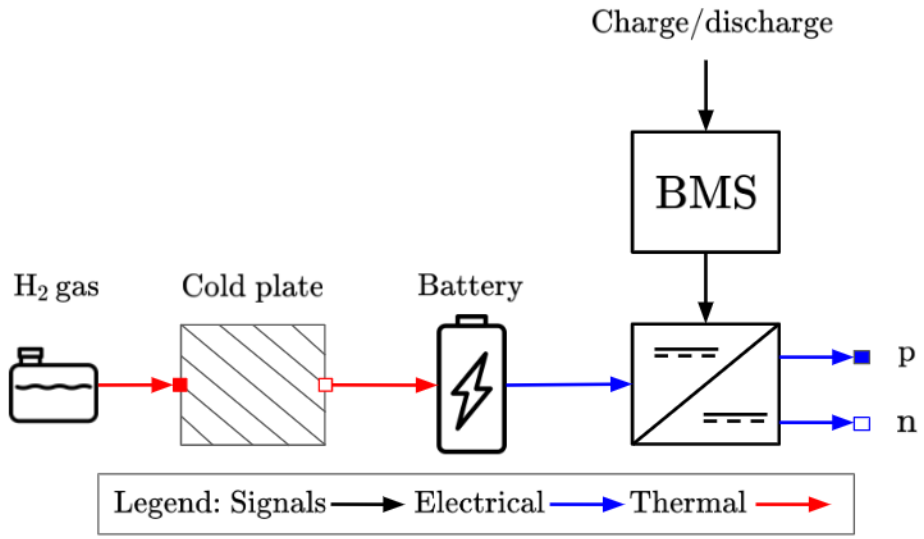

Fig. 11 Multi-domain schematic for the battery. The thermal connections are shown in red and the electrical connections are shown in blue.

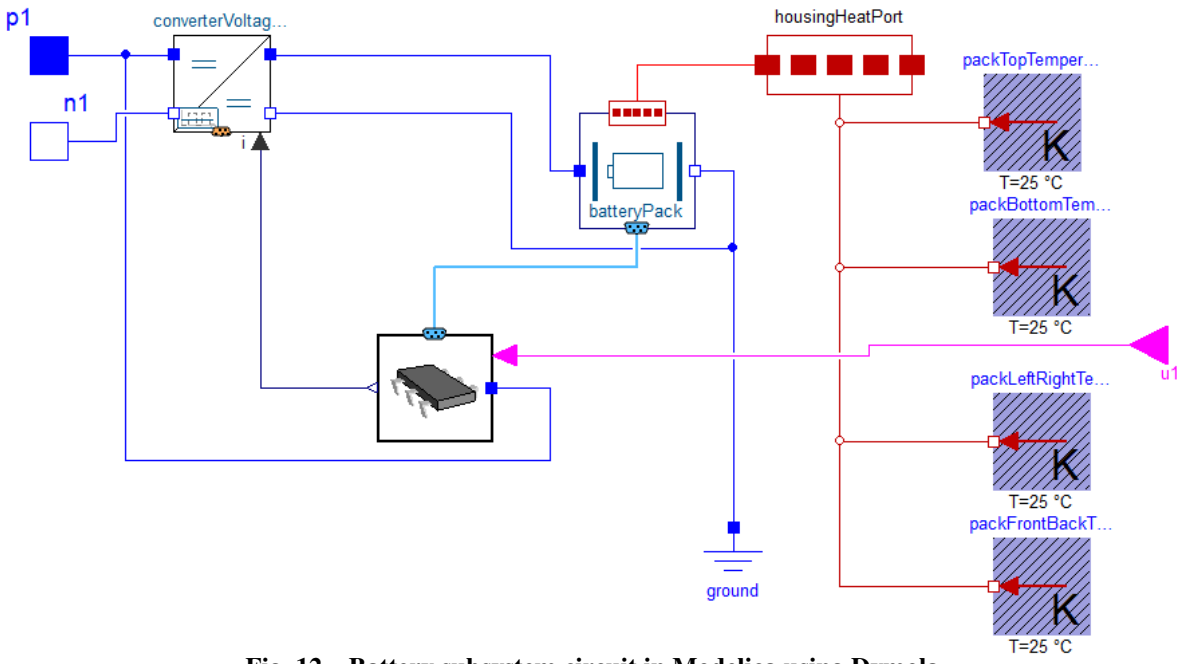

Fig. 12 Battery subsystem circuit in Modelica using Dymola.

consists of three domains: electrical (denoted by blue lines), thermal (denoted by red lines), and control (denoted by pink and light blue lines). There are three external connectors to link the model with the rest of the system: electrical connections `p1` and `n1` and Boolean control connection `u1`. The connector `u1` receives a signal from the main controller unit (MCU) to override the battery system in the event of electrical system failure. This control functionality would improve the safety, reliability, and resiliency of the aircraft's electrical system.

The battery model was developed using Modelica and the Dassault Battery [16]. The library uses [17],[18] to parameterize the battery models for various cell geometries and chemistries. In this case, the battery is parameterized according to the Sanyo 18650 Li-Ion battery provided in the library. The battery parameters are listed in Table 2. The housing model parameters are derived from the examples in the Battery Library [16] and the number of cells in series and parallel were determined from the CHEETA system requirements.

The current design for the battery subsystem is shown in Figure 13, which consists of a scaled pack of cylindrical cells with a Li-Ion chemistry. These scaling blocks, denoted by A and B in Figure 13, multiply the electrical and thermal characteristics of the individual Li-Ion `cell` block by the number of cells in parallel and series. The cold plate is required to maintain a constant temperature, and thus, this is modeled with a constant boundary condition that is applied to each side of the cell's housing through the `housingHeatPort` thermal connector in Figure 13. This port will then allow to determine the heat flow rate that the cold plate needs to absorb together with the liquid hydrogen cooling system to maintan a constant temperature, as illustrated in the top of Figure 14.

B. Model Validation and Simulation Studies

Before the battery management system and cold plate cooling system can be designed, the battery must be simulated to fully discharge to ensure that the discharge behavior is as expected. The battery is connected to three drivetrains as shown in Figure 14 and is configured in Dymola for simulation. This configuration represents one independent branch of the CHEETA electrical power system in Figure 1.

In this simulation scenario, the battery is run to completely discharge. The voltage and current are shown in Figure 15 and 16. The battery's state of charge over time is shown in Figure 17, which decreases linearly. However, since this battery model includes representation of non-ideal electrical behavior, the voltage decreases non-linearly over time as it discharges. The simulation terminates when the state of charge reaches 10%, this is part of the control logic in the BMS which aims to protect the battery health and prevent it from completely discharging.

The battery system is tested for different cold plate design and operating temperatures to give insight on how the thermal properties affect the battery's performance. The battery is placed in a circuit in Figure 18, which is modeled as

Table 2 Battery parameters.

Electrical Parameters		
Parameter	Description	Value
C_{nom}	Nominal capacity of the cells based on scaled data (As)	3600
n_p	Number of cells in parallel (unitless)	50
n_s	Number of cells in series (unitless)	125
SOC_{init}	Initial state of charge of the scaled pack (unitless)	1
T_b	Battery operating temperature (C)	20
V	Nominal voltage of battery (V)	500
Housing Model Parameters		
Parameter	Description	Value
D	Cell diameter (m)	0.0181
h	Cell height in z direction (m)	0.0648
$negDiameter$	Negative pin diameter (m)	0.009
$negHeight$	Positive pin height (m)	0.004
$posDiameter$	Positive pin diameter (m)	0.009
$posHeight$	Positive pin height (m)	0.004
t_s	Cell sheet thickness (m)	5e-5
N/A	Pin material	Steel
N/A	Sheet material	Steel
N/A	Core material	Lithium-Ion

a lumped thermal impedance with a constant temperature boundary condition imposed at all sides of the battery. The battery is connected in series with a variable resistor, which will change according to a step signal. The purpose of this test is to understand the effect of cold plate temperature on the electrical dynamics and internal resistances of the battery. The cold plate is configured to operate at three temperatures: 0° C, 20° C, and 40° C. Each battery has an initial cell temperature of 20° C.

The resistance in Figure 18 is stepped down from 10 Ω to 1 Ω at 10 seconds, which aims to emulate a change in the electrical load. The voltage and current produced by the battery at each temperature are shown in Figures 19 and 21. The temperature of the cold plate affects the current after the step, the severity of the peak current, and settling time of the current after the resistance drops. The internal resistance of the battery is shown in Figure 23, where the resistance drops during the transient period following the step change. The internal resistance is represented per cell in Figure 23, which would result in a large difference in battery losses when scaled to the specifications of the CHEETA aircraft. Lower cold plate temperatures results in higher ohmic internal resistances consistent with other studies such as [19]. These considerations are necessary to design the protections and control of the electrical system and battery management system.

VI. Conclusion

The objective of the CHEETA project was to develop a new design for fully-electrical commercial aircraft. Due to the envisioned use of hydrogen-based fuel and liquid cryogenic cooling, it was necessary to understand design trade-offs required to develop and validate multi-domain models (with different levels of modeling fidelity) for all subsystems in the proposed electric aircraft propulsion architecture. In this work, we created physics-based models of the battery and fuel cell systems and apply them to both the electrical and thermal studies. This modeling approach gives insight into the development of the aircraft system design and constraints.

The fuel cell system models are studied to understand the effects of temperature and sizing on the electrical and thermal behavior of the system. Because an actual commercially available fuel cell sized to the CHEETA specifications is not available yet, the system studies were conducted considering the capabilities of an existing smaller fuel cell to aid

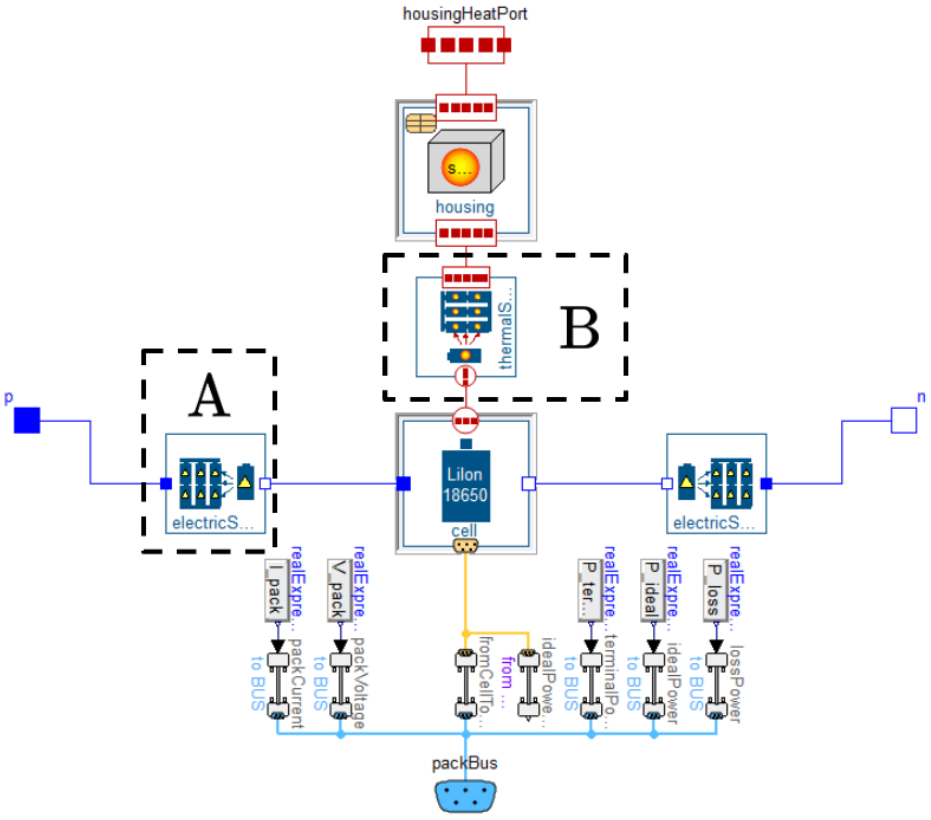

Fig. 13 Cylindrical scaled battery pack model from Dassault Battery Library.

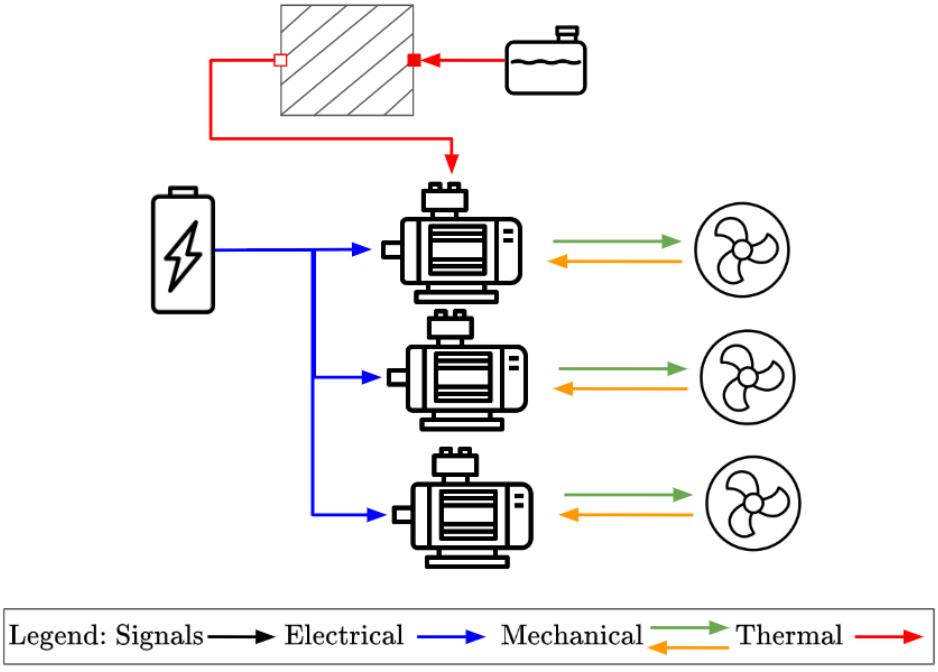

Fig. 14 Battery test circuit schematic.

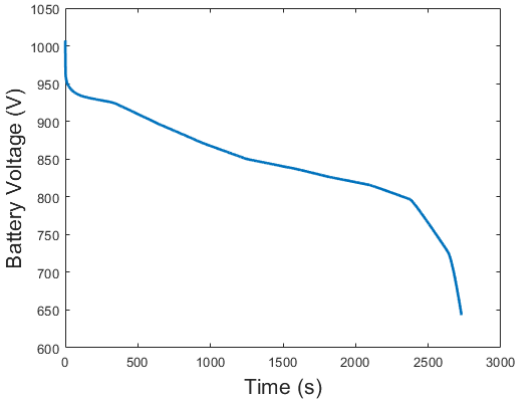

Fig. 15 Battery voltage during discharge test.

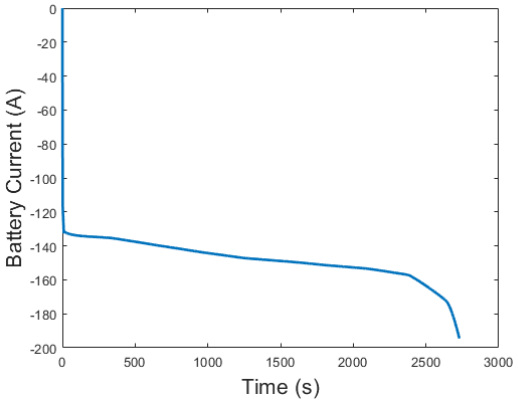

Fig. 16 Battery current during discharge test.

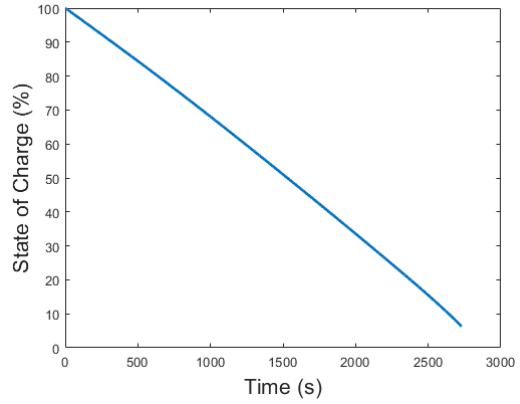

Fig. 17 Battery state of charge during discharge test.

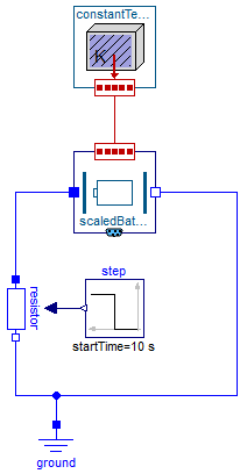

Fig. 18 Battery and cold plate system.

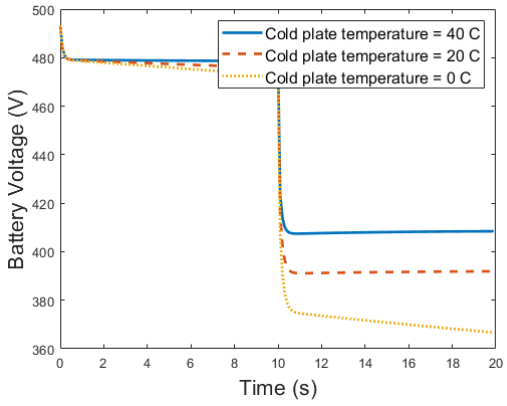

Fig. 19 Battery voltage during resistance step down test inset.

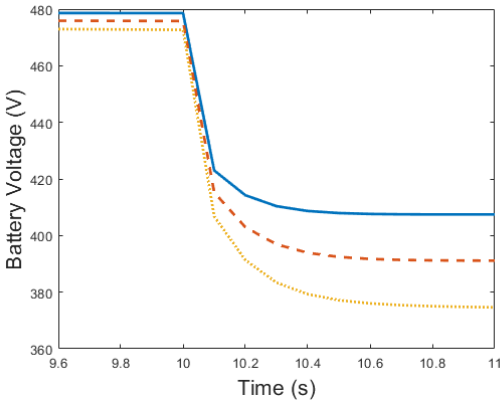

Fig. 20 Battery voltage during resistance step down test inset.

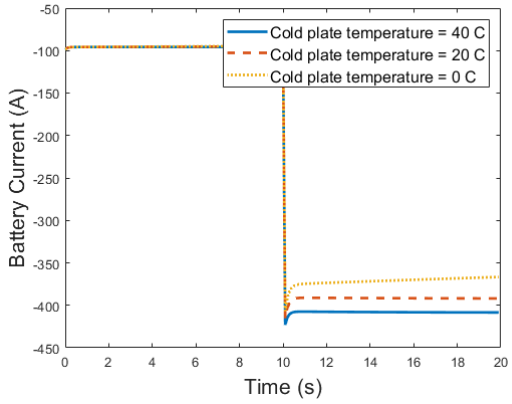

Fig. 21 Battery current during resistance step down test inset.

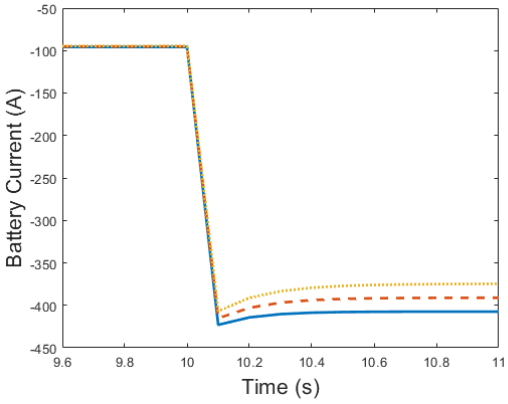

Fig. 22 Battery current during resistance step down test inset.

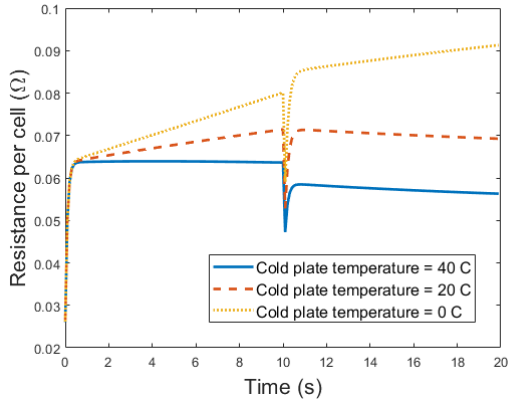

Fig. 23 Battery internal resistance per cell during resistance step down test inset.

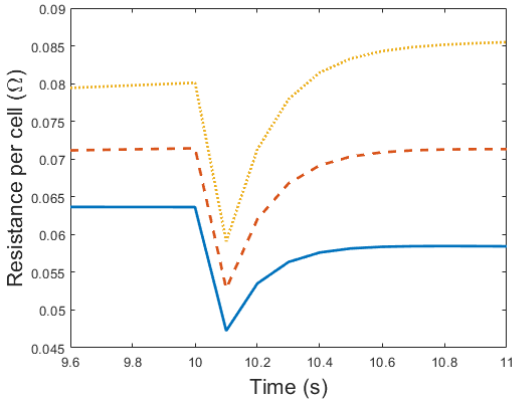

Fig. 24 Battery internal resistance per cell during resistance step down test inset.

in determining sizing for the subsystem. These tests provide understanding in scalability for fuel cell systems used in electric aircraft, showing the value of these integrated simulation studies at early stages of system development.

In the battery system, both requirements for the cold plate's design and battery management system were modeled and studied in the electrical, thermal, and control domains. This allows us to understand the effects of the operating temperature on the battery's losses and electrical dynamics to aid in the design of the multiple control schemes involved in the system (i.e., electrical management and protection, thermal management, etc.). The results of these studies provide a deeper understanding on how the cold plate temperature affects the electrical dynamics of the battery and the required heat flow rate that the cryogenic cooling system needs to be able to dissipate.

Acknowledgement

This work was supported in part by the National Aeronautics and Space Administration under award number 80NSSC19M0125 as part of the Center for High-Efficiency Electrical Technologies for Aircraft (CHEETA).

The work of M. Podlaski was supported by the National Science Foundation Graduate Research Fellowship Program under Grant No. DGE 1744655 and the Chateaubriand Fellowship of the Office for Science & Technology of the Embassy of France in the United States.

The work of L. Vanfretti was supported in part by Dominion Energy Virginia.

References

[1] Podlaski, M., Vanfretti, L., Khare, A., Nademi, H., Ansell, P., Haran, K., and Balachandran, T., "Initial Steps in Modeling of CHEETA Hybrid Propulsion Aircraft Vehicle Power Systems using Modelica," *2020 AIAA/IEEE Electric Aircraft Technologies Symposium (EATS)*, 2020, pp. 1–16.

[2] Lind, I., and Andersson, H., "Model Based Systems Engineering for Aircraft Systems - How does Modelica Based Tool Fit?" *Proceedings of the 8th International Modelica Conference*, Linköping Electronic Conference Proceedings, Vol. 63, Dresden, Germany, 2011, pp. 856–864.

[3] Hällqvist, R., Eek, M., Braun, R., and Krus, P., "Toward Objective Assessment of Simulation Predictive Capability," *Journal of Aerospace Information Systems*, Vol. 20, No. 3, 2023, pp. 152–167. https://doi.org/10.2514/1.I011153.

[4] Bals, J., Ji, Y., Kuhn, M., and Schallert, C., "Model Based Design and Integration of More Electric Aircraft Systems Using Modelica," *More Electric Aircraft Forum*, Barcelona, Spain, 2009.

[5] Batteh, J., Gohl, J., Sielemann, M., Sundstrom, P., Torstensson, I., MacRae, N., and Zdunich, P., "Development and Implementation of a Flexible Model Architecture for Hybrid-Electric Aircraft," *1st American Modelica Conference*, Boston, MA, USA, 2018, pp. 37–45. https://doi.org/10.3384/ecp1815437.

[6] Podlaski, M., Khare, A., Vanfretti, L., Sumption, M., and Ansell, P., "Multi-Domain Modeling for High Temperature Superconducting Components for the CHEETA Hybrid Propulsion Power System," *2021 AIAA/IEEE Electric Aircraft Technologies Symposium (EATS)*, 2021, pp. 1–10. https://doi.org/10.23919/EATS52162.2021.9704847.

[7] Waddington, E., Merret, J. M., and Ansell, P. J., "Impact of LH2 Fuel Cell-Electric Propulsion on Aircraft Configuration and Integration," *AIAA Aviation 2021 Forum*, 2021. Doi: 10.2514/6.2021-2409.

[8] Laraminie, J., and Dicks, A., "Proton Exchange Membrane Fuel Cells," *Fuel Cell Systems Explained*, Wiley, Hoboken, NJ, USA, 2003, pp. 67–119.

[9] Andersson, D., Åberg, E., Eborn, J., Yuan, J., and Sundén, B., "Dynamic modeling of a solid oxide fuel cell system in Modelica," *Proceedings of the 8th International Modelica Conference*, Linköping Electronic Conference Proceedings, Vol. 63, Dresden, Germany, 2011, pp. 593–602.

[10] Nehrir, M. H., and Wang, C., *Dynamic Modeling and Simulation of PEM Fuel Cells*, Wiley-IEEE, Hoboken, NJ, USA, 2009, pp. 57–84.

[11] Grumm, F., Schumann, M., Cosse, C., Plenz, M., Lücken, A., and Schulz, D., "Short Circuit Characteristics of PEM Fuel Cells for Grid Integration Applications," *Electronics*, Vol. 9, 2020, p. 602. Doi: 10.3390/electronics9040602.

[12] Modelica Association, "FMI Standard," 2023. https://fmi-standard.org/ (accessed April 11, 2023).

[13] Nehrir, M. H., and Wang, C., "Dynamic Models for PEMFCs and Tubular SOFCs," , 2023. URL https://ece.montana.edu/fuelcell/.

[14] Brück, D., Elmqvist, H., Mattsson, S. E., and Olsson, H., "Dymola for multi-engineering modeling and simulation," *Proceedings of modelica*, Vol. 2002, Citeseer, 2002.

[15] Li, S., and Ke, B., "Study of battery modeling using mathematical and circuit oriented approaches," *2011 IEEE Power Energy Soc. General Meeting (PESGM)*, 2011, pp. 1–8. Doi: 10.1109/PES.2011.6039230.

[16] Dassault Systemes, "CATIA Systems Battery Library," , 2015. https://www.3ds.com/fileadmin/PRODUCTS/CATIA/DYMOLA/PDF/3DS_2015_CATIA_BTY_Battery__Flyer_A4_WEB.pdf (accessed April 16, 2023).

[17] Schmalstieg, J., Käbitz, S., Ecker, M., and Sauer, D. U., "A holistic aging model for Li(NiMnCo)O2 based 18650 lithium-ion batteries," *J. of Power Sources*, Vol. 257, 2014, pp. 325–334. Doi: 10.1016/j.jpowsour.2014.02.012.

[18] Chen, M., and Rincon-Mora, G., "Accurate electrical battery model capable of predicting runtime and I-V performance," *IEEE Trans. Energy Convers.*, Vol. 21, No. 2, 2006, pp. 504–511. https://doi.org/10.1109/TEC.2006.874229.

[19] Yue, Y., Li, S., Cheng, X., Wei, J., Zeng, F., Zhou, X., and Yang, J., "Effects of temperature on the ohmic internal resistance and energy loss of Lithium-ion batteries under millisecond pulse discharge," *Journal of Physics: Conference Series*, Vol. 2301, IOP Publishing, 2022, p. 012014.